

Atomic and electronic structure of the Yb/Ge(111)-(3×2) surface studied by high-resolution photoelectron spectroscopy

M. Kuzmin,^{1,*} K. Schulte,² P. Laukkanen,¹ M. Ahola-Tuomi,¹ R. E. Perälä,¹ M. Adell,³
T. Balasubramanian,³ and I. J. Väyrynen¹

¹*Department of Physics, University of Turku, FIN-20014 Turku, Finland*

²*School of Physics and Astronomy, University of Nottingham, Nottingham NG7 2RD, United Kingdom*

³*MAX-lab, Lund University, SE-221 00 Lund, Sweden*

(Received 29 December 2006; published 6 April 2007)

Using high-resolution synchrotron-radiation photoelectron spectroscopy and low-energy electron diffraction, we have studied the electronic and structural properties of the Yb-induced Ge(111)-(3×2) reconstruction with a 1/6 monolayer coverage. We found these properties to be similar in many respects to those of the metal-induced Si(111) and Ge(111) reconstructions described previously in terms of the honeycomb chain-channel (HCC) structure. In particular, the Yb/Ge(111)-(3×2) is revealed to have a semiconducting character, the Yb atoms are divalent, and the surface states observed for the Yb/Ge(111) closely resemble those of the Na/Ge(111)-(3×1) in the literature. The Ge 3*d* core-level analysis, however, shows that the Ge 3*d* spectra from Yb/Ge(111)-(3×2) drastically differ from corresponding spectra of other Si and Ge HCC reconstructions. An atomic model, based on the general HCC geometry, is proposed for the Yb/Ge(111)-(3×2) surface. In this model, the important structural aspects are a buckling of the Ge=Ge double bond in the top, HCC-reconstructed layer plus a strong rearrangement of the second-layer atoms.

DOI: [10.1103/PhysRevB.75.165305](https://doi.org/10.1103/PhysRevB.75.165305)

PACS number(s): 68.35.-p, 68.43.Fg, 79.60.-i, 61.14.Hg

I. INTRODUCTION

Surface structures with reduced dimensionality have recently received significant attention in physics and technology because they exhibit fascinating properties and are considered potential materials for new nanodevices. For example, one-dimensional (1D) chainlike structures, produced by the adsorption of metal atoms (e.g., Au and In) on Si surfaces, have been extensively studied to observe and understand such exotic phenomena as Mott-Hubbard insulator,¹ non-Fermi-liquid ground states,² Peierls-type phase transitions,³ surface charge-density waves,^{3,4} and spin-charge separation.^{2,5}

Other interesting candidates for quasi-1D electron systems are low-coverage (3×*n*) (*n*=1, 2, and 4) surface phases induced by Ag, alkali metals (AMs), alkaline-earth metals (AEMs), and rare-earth metals (REMs) on Si(111) and Ge(111). On the basis of transmission electron diffraction,⁶ surface x-ray diffraction data,⁷ and density-functional theory (DFT) calculations,^{8,9} the most plausible model for the AM/ and Ag/Si(111)-(3×1) surfaces has been proposed to be the honeycomb chain-channel (HCC) structure shown in Fig. 1(a). In this structure, the first-layer Si atoms *a*, *b*, *c*, and *d* rearrange to form (i) the nearly planar honeycomb chains with unusual Si(*b*)=Si(*c*) double bonds and (ii) the empty channels that accommodate 1/3 monolayer (ML) of metal atoms adsorbed at the *T*4 sites. According to DFT calculations in Refs. 8 and 9, such a structure is not only energetically favored but also accurately reproduces scanning-tunneling-microscopy (STM) images, surface-state band dispersions in angle-resolved photoelectron spectroscopy (ARPES), and surface core-level shifts (SCLSs) in Si 2*p* core-level spectra. Moreover, the HCC geometry aptly describes the semiconducting character of the AM/Si(111)-(3×1) surfaces¹⁰ as well as the Si atom density (4/3 ML)

determined for Na/Si(111)-(3×1).¹¹ More generally, a similar HCC structure was also found to be the ground-state atomic configuration for related Na/, Li/, and K/ Ge(111)-(3×1) surfaces, as evidenced by the total energy calculations in Ref. 12, and adequately explains the STM images in Refs. 13–15.

For the AEM/ and REM/Si(111)-(3×2) phases, the Si surface has been proposed to have the same HCC reconstruction as for the AM/Si(111)-(3×1) phases.^{16–28} The metal coverage of the (3×2)-AEM and -REM phases, however, is 1/6 ML rather than 1/3 ML; that is, the AEM and REM atoms occupy every second *T*4 site in the (3×2) HCC, while the other *T*4 sites are empty, as illustrated in Fig. 1(b). [Note that, in the case of the adsorption of Mg on Si(111), the *H*3 site is slightly more stable than *T*4.²⁹] As predicted by *ab initio* calculations^{16,18,19,29} and supported by STM (Refs. 16, 18, and 19) and SCLS measurements (Refs. 22 and 25–27), this difference leads to a slight deformation of neighboring Si honeycombs in the equilibrium (3×2) HCC structure in Fig. 1(b): the left edge of the honeycomb chain in Fig. 1(b) exhibits a lateral corrugation (i.e., the adjacent *a* and *a'* atoms are displaced in the direction perpendicular to the chain) and the right edge exhibits a pairing of the *d* atoms due to the Coulomb interaction between the metal ion and the dangling-bond electrons of the surrounding Si. Hence, for both the equilibrium HCC structures of 1/3 ML (3×1) and 1/6 ML (3×2) Si surfaces in Figs. 1(a) and 1(b), the metal atoms are adsorbed at the equivalent (*T*4) sites, and therefore, these models are referred to as *T*4 HCC models. In contrast, the HCC reconstruction induced by 1/6 ML Eu on Ge(111) was found to have two distinct adsorption sites for the metal atoms.^{30,31} This reconstruction shows the microscopically mixed (3×2) and (3×4) periodicities in STM images,³⁰ and a so-called *T*4*H*3 model, where the Ge substrate has the basic HCC configuration and the Eu atoms are adsorbed at *T*4

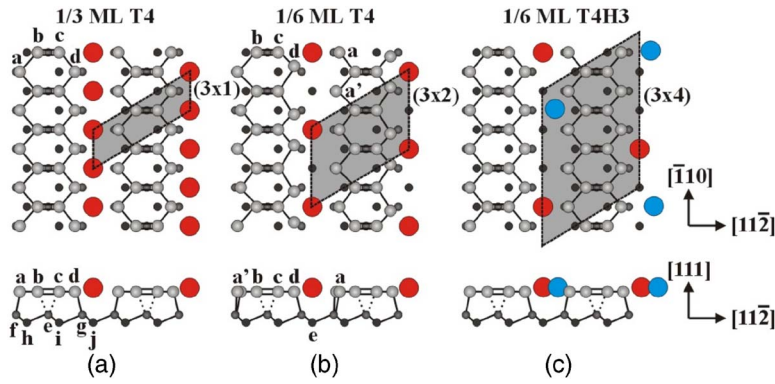


FIG. 1. (Color online) Atomic configurations of (a) the $1/3$ ML (3×1) reconstruction induced by AM on Si(111) and Ge(111), (b) the $1/6$ ML (3×2) reconstruction induced by AEM and REM on Si(111), and (c) the $1/6$ ML $(3 \times 2)/(3 \times 4)$ reconstruction induced by Eu on Ge(111). The metal atoms (large circles) are adsorbed on $T4$ sites in (a) and (b), and occupy both $T4$ and $H3$ sites in (c). The (3×1) , (3×2) , and (3×4) unit cells are marked.

and $H3$ [see Fig. 1(c)], was proposed for the Eu/Ge(111)- $(3 \times 2)/(3 \times 4)$ surface based on STM, Eu $4f$ and Ge $3d$ core-level analyses.³¹

When comparing Si and Ge HCC reconstructions, STM and ARPES results are highly similar; however, Si $2p$ and Ge $3d$ core-level data show significant differences for these two systems. In particular, the Si $2p$ spectra from the AM/Si(111)- (3×1) phases typically show two surface components shifted to lower and higher binding energies (BEs) relative to the bulk emission peak.^{9,32–35} In contrast, although Ge $3d$ spectra from K/ (Ref. 36) and Na/Ge(111)- (3×1) (Ref. 37) do reveal two surface components, both appear on the lower BE side. The Li/Ge(111)- (3×1) surface even gives rise to only one surface component at lower BE.³⁸ For the $1/6$ ML HCC reconstructions, three Si $2p$ surface components were identified for the Ca/²² Ba/²⁷ Yb/³⁹ Sm/⁴⁰ and Eu/Si(111)- (3×2) (Refs. 25 and 26) surfaces. The surface components found in the Ge $3d$ spectra from the Eu/Ge(111)- $(3 \times 2)/(3 \times 4)$ reconstruction are qualitatively similar to those of the Si $2p$ spectra from the Si (3×2) surfaces.³¹ However, the intensity ratios of the Ge $3d$ surface components differ dramatically from those of the Si-based reconstructions. For this reason, the atomic structure of the Eu/Ge(111)- $(3 \times 2)/(3 \times 4)$ was assumed to be different from that of the AEM/ and REM/Si(111)- (3×2) surfaces. All in all, the interpretation of the Si $2p$ and Ge $3d$ spectra for the Si and Ge HCC reconstructions is still not fully resolved, and hence it is unclear to what extent the Si and Ge reconstructions can be considered similar.

In this study, we have investigated the structural and electronic properties of an Yb/Ge(111)- (3×2) surface at the coverage of $1/6$ ML by low-energy electron diffraction (LEED) and high-resolution photoelectron spectroscopy using synchrotron radiation. The paper is organized as follows. The experimental details are given in Sec. II. The LEED, valence-band, and Yb $4f$ and Ge $3d$ core-level results are presented in Sec. III. Finally, we analyze these data and discuss similarities and differences between our Yb/Ge(111)- (3×2) and related AM/, AEM/, and REM/Si(111) and /Ge(111) surfaces in terms of the HCC structure model.

II. EXPERIMENT

The experiments were performed in beamline 33 at the MAX-lab synchrotron radiation laboratory in Lund, Swe-

den.⁴¹ The photoemission measurements were carried out in ultrahigh vacuum below 10^{-10} Torr at room temperature (RT) using linearly polarized synchrotron radiation light and an angle-resolved photoelectron spectrometer ARUPS10 with an angular resolution of $\pm 2^\circ$. The photon incidence angle (θ_i) was fixed at 45° from the surface normal, and the photoelectron emission angle (θ_e) was varied by the rotation of an analyzer in the plane defined by the photon incidence direction and the surface normal (see the schematic drawing in Fig. 5). The total energy resolution was around 75 meV at photon energies ($h\nu$) of 21.2 and 23 eV, between 80 and 100 meV at $h\nu=70$ and 95 eV, and on the order of 300 meV at $h\nu=150$ and 175 eV in the valence-band, Ge $3d$, and Yb $4f$ measurements, respectively. The BE was referred to the Fermi level (E_F) of a Ta foil mounted on the sample holder in good electrical contact with the Ge substrate.

The Ge samples were cut from a Sb-doped (n -type) (111) wafer. Sample cleaning was carried out by repeated cycles of 1.0 keV Ar⁺ sputtering at 673 K and subsequently annealing the sample at 900 K until an excellent $c(2 \times 8)$ LEED pattern with sharp fractional-order spots and a low background [Fig. 2(a)] was displayed. The sample heating was performed by direct current. Temperature was measured by an infrared pyrometer. Yb was deposited from a W-filament evaporator onto the clean Ge(111) substrate at RT, followed by annealing at 700 K for several minutes to produce a long-range order on the surface. The deposition rate was about 0.45 ML/min [1 ML is referred to as the atomic density on the bulk-terminated Ge(111) surface: 7.22×10^{14} atoms/cm²], as estimated by a quartz crystal microbalance. In addition, the Yb deposition rate was checked using a separate Si(111) sample, for which the Yb-induced LEED superstructure was monitored as a function of the deposition time, taking into account the earlier LEED observations.⁴²

III. RESULTS

A. LEED

Figure 2(b) represents a LEED pattern of the Yb/Ge(111) surface at the coverage of $1/6$ ML. This surface shows (3×1) spots, which strongly resemble the LEED observations for the $1/6$ ML AEM/ and REM/Si(111)- (3×2) surfaces in Refs. 11, 20, and 43. For those reconstructions, the (3×1) LEED periodicity has been shown to originate from the Si geometry, whereas the adsorbate subsystem has the

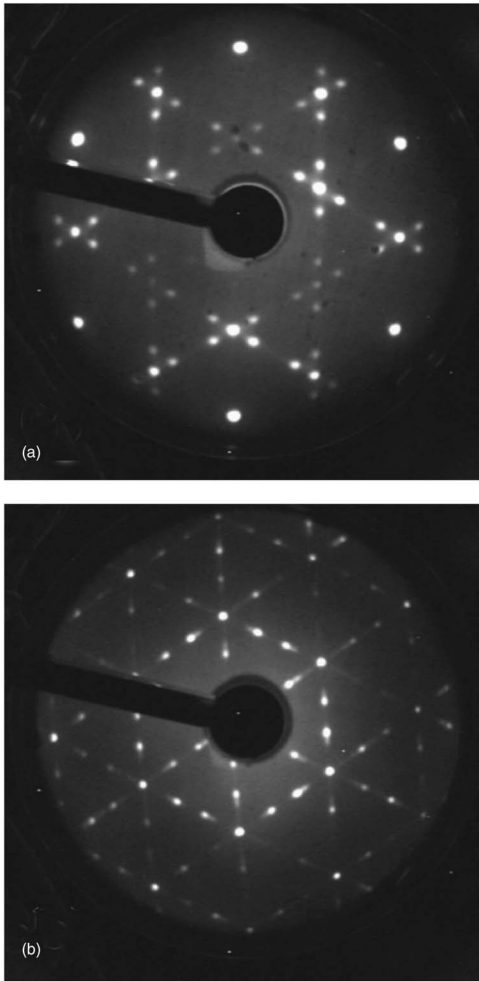


FIG. 2. LEED patterns of (a) the clean Ge(111)- $c(2 \times 8)$ surface and (b) the Yb/Ge(111)- (3×2) surface at a coverage of $1/6$ ML. The electron energies are (a) 36 eV and (b) 100 eV.

actual (3×2) periodicity and the appearance of respective half-order LEED features (in most cases, faint streaks) depends on the degree of the adsorbate-row correlation⁴⁴ and on the electron energy.²⁵ We therefore propose that the actual periodicity of the $1/6$ ML Yb/Ge(111) reconstruction is (3×2) , and we will refer to this surface as the Yb/Ge(111)- (3×2) hereafter. Note that the Eu/Ge(111) reconstruction with a $1/6$ ML coverage also showed the (3×1) LEED periodicity, but STM revealed both the overall (3×2) as well as localized (3×4) periodicities for this surface.³⁰ In this study, however, we do not have evidence for the (3×4) periodicity, and hence will not consider such a periodicity for the Yb/Ge(111) surface.

We also remark that dim oblong LEED features can be discerned in the vicinity of the $1/3$ -order spots in Fig. 2(b). Because the positions of these features are inconsistent with the (5×1) LEED pattern, they cannot be interpreted as due to the (5×1) or (5×2) structure observed for the AEM/ and REM/Si(111) surfaces at a higher coverage than $1/6$ ML. Rather, it is believed that the origin of the oblong features in Fig. 2(b) is the splitting of the (3×1) LEED spots, caused by the limited domain size of the Yb/Ge(111)- (3×2) recon-

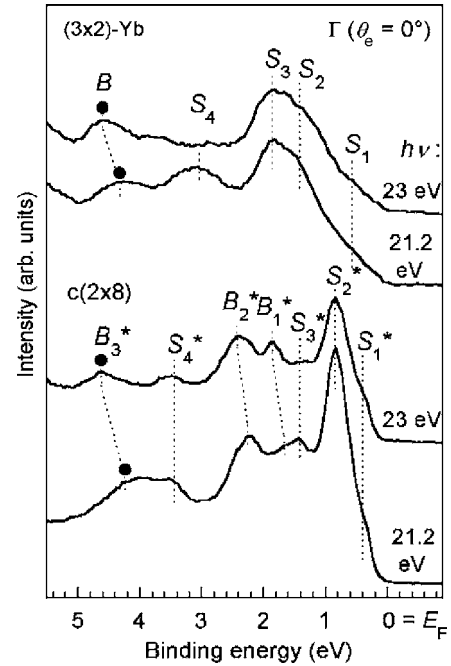


FIG. 3. Valence-band spectra of the Ge(111)- $c(2 \times 8)$ and Yb/Ge(111)- (3×2) surfaces, taken at $\theta_e = 0^\circ$ and $h\nu = 21.2$ and 23 eV. The bulk- and surface-related states are denoted by “B” and “S,” respectively.

struction in the direction of threefold periodicity (i.e., along the $[11-2]$ direction). We can infer this from a similar splitting observed for a single-domain (3×2) phase induced by Yb on a vicinal Si(111) surface, tilted 4° towards the $[-1-12]$ direction, where the (3×2) -domain dimension was strongly confined in the $[11-2]$ direction by limited terrace widths.⁴⁵

B. Valence-band spectra

Since the Ge(111)- $c(2 \times 8)$ and Yb/Ge(111)- (3×2) are triple-domain surfaces, there is an ambiguity in interpreting ARPES spectra from such structures at finite k_{\parallel} (where k_{\parallel} is the momentum parallel to the surface). At $k_{\parallel} = 0$, however, the contributions from three different domains are identical. For this reason, we measured valence-band spectra only at normal emission, $\theta_e = 0^\circ$, which corresponds to the $\bar{\Gamma}$ symmetry point ($k_{\parallel} = 0$). Figure 3 presents the spectra taken at photon energies $h\nu = 21.2$ and 23 eV for both surfaces. For the Ge(111)- $c(2 \times 8)$, several emission features (labeled $S_1^* - S_4^*$ and $B_1^* - B_3^*$) are found. Since none of these features lie in the band gap at the $\bar{\Gamma}$ point,⁴⁶ they cannot directly be assigned to surface states. However, some of the features were identified as surface states in earlier ARPES studies.⁴⁷⁻⁵² In particular, the peak S_2^* at 0.85 eV below E_F , which is the dominant feature in both of the $c(2 \times 8)$ spectra, agrees well with those studies, where it was assigned to the rest-atom dangling-bond surface state. Also, the feature S_3^* at the BE of 1.4 eV was observed in Refs. 47-52, where it was connected with the adatom back-bond surface state. Moreover, the weak shoulder S_1^* is due to the back-bond surface states localized

in the first layer, with some weight in the second layer, as shown in the *ab initio* study.⁵³ Note that the energy positions of S_1^* , S_2^* , and S_3^* do not change between $h\nu=21.2$ and 23 eV, supporting their surface-state characters.

Regarding the other features in the spectra for Ge(111)- $c(2\times 8)$, most of them are related to bulk bands because such features were found to persist upon an exposure of atomic hydrogen.⁴⁸ In fact, the B_1^* , B_2^* , and B_3^* are dispersive at $h\nu=21.2$ and 23 eV, and therefore, they are suggested to be due to the direct bulk transitions. In contrast, the S_4^* can be related to the surface structure (e.g., surface resonance or umklapp process). A similar feature was previously found in Ref. 48, where it disappeared upon an exposure of atomic hydrogen. Thus the spectra of the clean surface in Fig. 3 agree well with earlier ARPES studies.

For the Yb/Ge(111)- (3×2) surface, the valence-band spectra are drastically modified. As illustrated in Fig. 3, the (3×2) spectrum at $h\nu=21.2$ eV shows at least five features at BE=0.55, 1.5, 1.85, 3.1, and 4.3 eV (labeled S_1 , S_2 , S_3 , S_4 , and B , respectively). The S_1 , S_2 , and S_3 features have the same BEs at $h\nu=23$ eV and are not observed for the clean surface. We can therefore assume that the S_1 , S_2 , and S_3 are related to new surface states of the Yb/Ge(111)- (3×2) reconstruction. In contrast, the B feature corresponds directly to the bulk feature B_3^* of the clean surface. The S_4 feature, which can be readily identified in the spectrum at $h\nu=21.2$ eV but not in the spectrum at $h\nu=23$ eV, does not show a one-to-one correspondence with the clean surface. Most likely, this feature is due to the second-order light ($h\nu=42.4$ eV) and is related to the Yb $5p_{3/2}$ core level.

C. Yb 4f emission

It is well known that the valence state of Yb atoms depends on their surroundings. Therefore, the Yb valence can be an important criterion when constructing a structural model for the Yb/Ge(111)- (3×2) reconstruction. It can be easily determined from Yb 4f photoemission spectra where the $4f^{13}$ and $4f^{12}$ final states, which are due to the divalent and trivalent configurations of Yb atoms, respectively, are well separated in energy.⁵⁴ Figure 4 shows the Yb 4f spectrum measured with normal emission angle, taken at a photon energy of 175 eV, where the Yb 4f emission is strongly enhanced. The Yb 4f spectrum shows only a doublet of spin-orbit split peaks at BE=1.49 and 2.76 eV, which correspond to divalent Yb atoms (i.e., $4f^{13}$ final state). In contrast, no features are discerned between 4 and 11 eV, where the Yb $4f^{12}$ final-state multiplet is expected to be observed. We therefore conclude that the Yb atoms are completely divalent in the Yb/Ge(111)- (3×2) reconstruction. No emission is found at the Fermi level in Figs. 3 and 4, indicating that the Yb/Ge(111)- (3×2) surface is semiconducting. The observed electronic properties of the Yb/Ge(111)- (3×2) agree well with those of the Eu/Ge(111)- $(3\times 2)/(3\times 4)$, and those of the AEM/ and REM/Si(111)- (3×2) reconstructions with the HCC geometry.

The inset of Fig. 4 depicts the Yb 4f spectrum of the Yb/Ge(111)- (3×2) in more detail. As shown, the Yb²⁺ state of this spectrum can be reasonably reproduced by a single

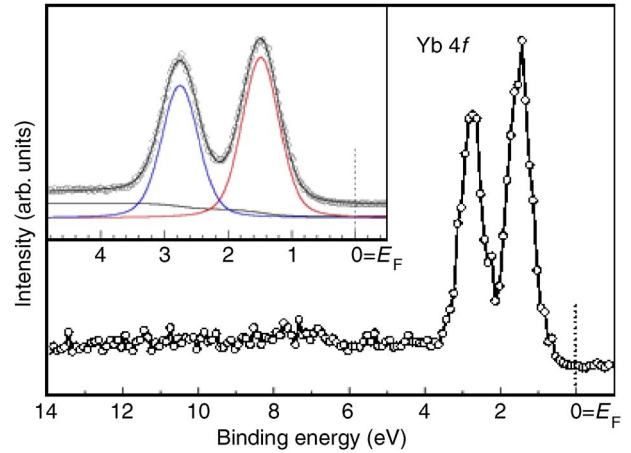


FIG. 4. (Color online) Yb 4f spectrum of the Yb/Ge(111)- (3×2) surface taken at $h\nu=175$ eV and normal emission. The inset shows the fitting of Yb $4f^{13}$ final-state feature, recorded at $h\nu=150$ eV, by a single doublet with the Voigt functions. The background is removed by Shirley's method.

doublet of Voigt functions. The spin-orbit splitting is found to be 1.269 eV, agreeing well with earlier fitting data for the Yb 4f spectra (e.g., see Ref. 55). The branching ratio is 1.21, which is somewhat different from the theoretical value of 4/3, but can be accounted for by diffraction effects.⁵⁶ The Lorentzian width (LW) and Gaussian width (GW) are found to be 0.172 and 0.588 eV, respectively. The presence of only one component in the Yb 4f spectrum suggests that the Yb atoms reside at equivalent adsorption sites in the Yb/Ge(111)- (3×2) reconstruction. Their precise origin will be discussed in Sec. IV.

D. Ge 3d core level

The Ge 3d core-level spectra were taken with varying surface and bulk sensitivities by using different photon energies and emission angles. Figure 5 presents normalized spectra from the Yb/Ge(111)- (3×2) surface. In addition, in order to verify the fitting procedure and extract some of the fitting parameters, we also measured the Ge 3d spectra of the clean Ge(111)- $c(2\times 8)$ surface, which were previously deconvoluted and described in detail.⁵⁷ A spectrum from the clean surface, taken at $(h\nu, \theta_e)=(95$ eV, $0^\circ)$, is shown at the bottom of Fig. 5. This spectrum is fitted by one bulk (B) and three surface ($S1'$, $S2'$, and $S3'$) components. The raw data are represented by open circles and the resulting fitting curve by a solid line. The individual bulk and surface components are plotted below the raw spectrum. The decomposition was made by using a standard least-squares-fitting procedure with a linear combination of spin-orbit split Voigt functions. The background (solid line below the spectrum) was removed by Shirley's method. The fitting parameters are given in Table I. Clearly, these results are in close agreement with those in earlier studies.^{31,57} The atomic origins of $S1'$, $S2'$, and $S3'$ are considered to be pedestal (first-layer) atoms, half of the rest atoms, and adatoms of the $c(2\times 8)$ structure, respectively.

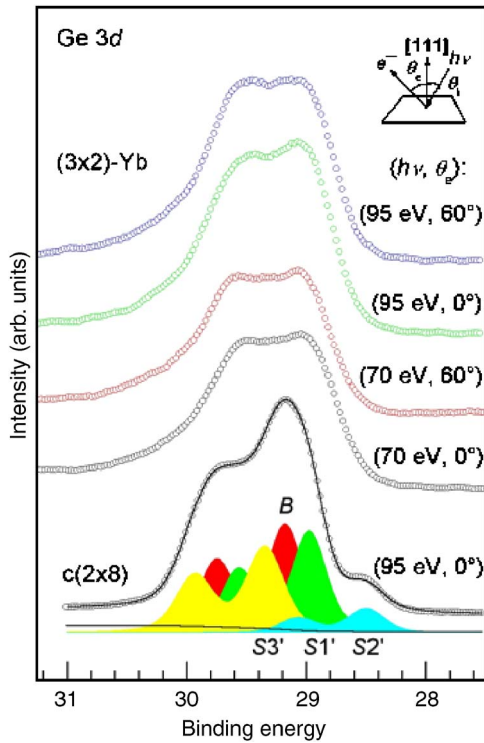


FIG. 5. (Color online) Ge $3d$ core-level spectra of the Eu/Ge(111) taken at various photon energies ($h\nu$) and emission angles (θ_e). The bottom spectrum is obtained for the clean Ge(111)- $c(2 \times 8)$ surface at $h\nu=95$ eV and $\theta_e=0^\circ$. This spectrum is decomposed into the bulk component (B) and three surface components ($S1'$ – $S3'$), which are represented by shadowed doublets below the raw data (open circles). The background (solid line) is removed by Shirley's method. At the upper right, a schematic drawing illustrates the geometry of experiment. The fitting parameters are presented in Table I.

The Ge $3d$ spectra of the Yb/Ge(111)- (3×2) surface are clearly different from those of the clean surface. First, the two spin-orbit split Ge $3d_{3/2}$ and $3d_{5/2}$ structures are now less pronounced. This suggests that the (3×2) reconstruction involves a larger number of different surface and/or subsurface Ge atoms than the clean $c(2 \times 8)$ reconstruction. Second, the higher BE sides of the (3×2) spectra trail off more gently than that of the $c(2 \times 8)$ spectrum. This infers that the $(3$

TABLE I. Fitting parameters for the Ge $3d$ core-level spectrum of the Ge(111)- $c(2 \times 8)$ surface, taken at $h\nu=95$ eV and $\theta_e=0^\circ$. The spectrum is deconvoluted by the bulk component (B) and three surface components ($S1'$ – $S3'$). The spin-orbit splitting and surface core-level shifts are given in eV. The Lorentzian and Gaussian widths are in meV.

	B	$S1'$	$S2'$	$S3'$
Spin-orbit splitting		0.58		
Branching ratio		1.57		
Lorentzian width		150		
Gaussian width	265	269	275	287
Surface core-level shift		-0.21	-0.70	0.18

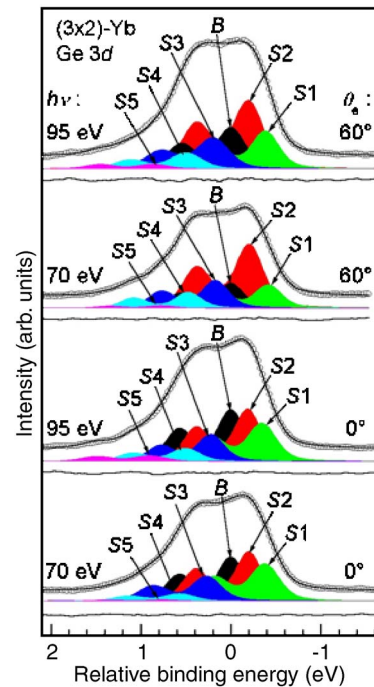


FIG. 6. (Color online) Decomposition of Ge $3d$ spectra from the Yb/Ge(111)- (3×2) . The experimental data are shown by open circles. The fitting curves are shown by solid lines. The bulk (B) and surface ($S1$ – $S5$) components are indicated by shadowed doublets. The residual between the experimental and fitting results is given at the bottom of each spectrum. The binding energy is referenced to the bulk component.

$\times 2$) spectra include more than one surface component at higher BE relative to the bulk emission. Finally, we emphasize that the (3×2) spectra do not show the characteristic shoulder at lower BE, which is clearly observed in the $c(2 \times 8)$ spectrum and which is mainly caused by rest atoms (the component $S2'$). Therefore, the Yb adsorbate fully removes the $c(2 \times 8)$ structure on the Ge(111) surface, agreeing well with the present LEED and valence-band results.

More information can be obtained by decomposing the Ge $3d$ spectra of the (3×2) surface as depicted in Fig. 6. The fitting procedure was similar to that of the clean spectrum described above. The spin-orbit splitting and LW were the same as for the clean spectrum, and were kept constant for all spectra. The GW was allowed to vary for different photon energies because of the dependence of the energy resolution on $h\nu$. In a similar way, the branching ratio was allowed to vary slightly due to diffraction effects.⁵⁶ The SCLSs were allowed to vary freely, yet were required to give the same energy positions in all spectra. Applying the above constraints, we first tried a fitting scheme with one bulk and three surface components. Within this scheme, the fitting curves could not reproduce the experimental spectra satisfactorily, especially towards the high-binding-energy side. Introducing a fourth surface component, dramatically improved the quality of the fit. However, the high BE trail of the (3×2) spectra could still not be fitted adequately. Introducing a fifth surface component resulted, finally, in an accurate fit of the (3×2) spectra, including their high BE sides. The

TABLE II. Fitting parameters for the Ge $3d$ spectra of the Yb/Ge(111)-(3 \times 2) surface (Fig. 6) decomposed by using the bulk component B and five surface components $S1$ – $S5$. The spin-orbit splitting and surface core-level shifts are given in eV, and the Lorentzian and Gaussian widths are in meV.

	B	$S1$	$S2$	$S3$	$S4$	$S5$
Spin-orbit splitting			0.58			
Branching ratio			1.60 \pm 0.01			
Lorentzian width			150			
Gaussian width at $h\nu=70(95)$ eV	265(275)	273(282)	0.281(289)	289(301)	292(304)	290(302)
Surface core-level shift		–0.19	–0.38	0.22	0.52	0.82

fitting parameters for the (3 \times 2) spectra are presented in Table II. The surface components $S1$ and $S2$ are shifted to lower BE, and $S3$, $S4$, and $S5$ to higher BE relative to the bulk component B . Analyzing the relative intensities of the components, we find that the intensity of $S5$ is always quite low and ranges from $S5/B=0.03$ at $(h\nu, \theta_e)=(70 \text{ eV}, 0^\circ)$ to $S5/B=0.12$ at $(h\nu, \theta_e)=(95 \text{ eV}, 0^\circ)$. We therefore argue that the $S1$ – $S4$ components are related to the Ge bonding sites in the Yb/Ge(111)-(3 \times 2) reconstruction, while the $S5$ originates from defects, disorder, contaminations, etc., in the surface and/or subsurface area. (Note that heavy carbon and oxygen contaminations would result in a trivalent multiplet in the Yb $4f$ emission,⁵⁵ which was not found in the Yb $4f$ spectrum of Fig. 3.) The intensity ratios of $S1/B$, $S2/B$, $S3/B$, and $S4/B$ increase at both $h\nu$ when changing the emission angle from $\theta_e=0^\circ$ to $\theta_e=60^\circ$, i.e., increasing the surface sensitivity, as expected. Between the $S1$ and $S4$ components, however, the behavior of $S1$ is different from the other three. In going from $\theta_e=0^\circ$ to $\theta_e=60^\circ$, the intensity ratio of $S1/B$ increases by only $\sim 10\%$, whereas the $S2/B$, $S3/B$, and $S4/B$ ratios increase by ~ 80 – 200% . We therefore interpret the $S1$ as arising from subsurface atoms and the $S2$ – $S4$ from the topmost atoms of the (3 \times 2)-Yb.

IV. DISCUSSION

The valence-band surface states S_1 – S_3 observed for the Yb/Ge(111)-(3 \times 2) in Sec. III B are found to be very similar to those of the Na/Ge(111)-(3 \times 1) surface taken at normal emission.^{37,58} Hence, we speculate that the Ge structures of 1/6 ML Yb/Ge(111)-(3 \times 2) and 1/3 ML Na/Ge(111)-(3 \times 1) will have similar geometric properties. The *ab initio* study¹² showed that the atomic structure of the Na/Ge(111)-(3 \times 1) can be understood in terms of the 1/3 ML HCC model in Fig. 1(a). We therefore assume that the substrate structure of the Yb/Ge(111)-(3 \times 2) can also be interpreted within the related HCC geometry. In addition, we emphasize that, according to the present Yb $4f$ data, the Yb atoms are divalent and the Yb/Ge(111)-(3 \times 2) surface is semiconducting (Sec. III C). These facts are also supportive of the HCC structure with a 1/6 ML coverage for the Yb/Ge(111)-(3 \times 2) reconstruction.

Next, we discuss the Ge $3d$ core-level data (Sec. III D) as compared to previous Si $2p$ and Ge $3d$ results for the (3 \times 1) and (3 \times 2) HCC reconstructions.^{9,22,25–27,32–40} We find

that the Ge $3d$ core-level emission from the Yb/Ge(111)-(3 \times 2) reconstruction includes two lower BE components $S1$ (with an SCLS of -0.19 eV) and $S2$ (-0.38 eV) and two higher BE components $S3$ (0.22 eV) and $S4$ (0.52 eV) (Fig. 6). $S2$ – $S4$ are connected with the top-layer atoms and $S1$ with the subsurface atoms of the reconstruction. Hence the number of Ge $3d$ surface components for the Yb/Ge(111)-(3 \times 2) is different from that of the Eu/Ge(111)-(3 \times 2)/(3 \times 4) (Ref. 31) as well as from the number of Si $2p$ surface components for the AEM/ and REM/Si(111)-(3 \times 2).^{22,25–27,39,40} This means that, despite the common, overall HCC geometry, the detailed atomic arrangement of the Yb/Ge(111)-(3 \times 2) should be subtly different from those of the Eu/Ge(111)-(3 \times 2)/(3 \times 4) and Si (3 \times 2) HCC structures in Figs. 1(c) and 1(b), respectively.

Figure 7 depicts an atomic configuration which is a possible candidate to account for all the present results for the Yb/Ge(111)-(3 \times 2) reconstruction within the basic HCC framework. The top layer of this structure is formed by the a , b , c , and d honeycomb-chain Ge atoms and the Yb atoms with a 1/6 ML coverage, which arrange the $\times 2$ rows in the empty channels between the Ge honeycomb chains. We then place the Yb atoms on $T4$ sites, since (i) the Yb $4f$ measurements show a single adsorption site for the Yb atoms (Sec. III C) and (ii) $T4$ and $H3$ are the most favorable adsorption sites in (3 \times 2) HCC structures, with the surface energy of the $T4$ site usually slightly lower than that of the latter [e.g., by 0.01, 0.07, 0.08, and 0.09 eV/(3 \times 2) for Ba,¹⁸ Sm,¹⁹ Sr,²⁹ and Ca²⁹ on Si(111)]. The outer atoms of the Ge honeycomb chains (i.e., a and d in Fig. 7) are expected to gain more

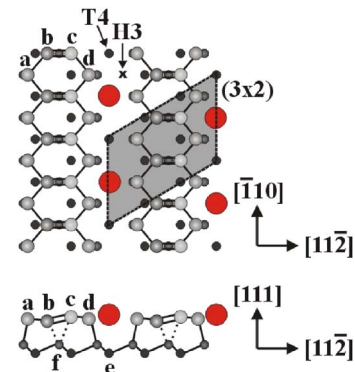


FIG. 7. (Color online) A structural model proposed for the Yb/Ge(111)-(3 \times 2) surface. See the text for details.

electron charge as they have dangling-bond orbitals and can therefore interact with the Yb atoms, which donate two electrons per (3×2) unit. Among the purely surface-related Ge $3d$ components, only $S2$ has a negative core-level shift. Hence we propose that the atomic origin of $S2$ are the a and d atoms in Fig. 7. At present, we depict the outer honeycomb-chain atoms as equivalent within our assignment, as is the case for the AM/Si(111)- (3×1) surfaces with only one negatively shifted component in their Si $2p$ spectra.^{9,35} Any possible difference in binding energies between the a and d atoms in the Yb/Si(111)- (3×2) appears to be too small to be resolved in the present study.

The components $S3$ and $S4$ with positive core-level shifts can be associated with the inner honeycomb-chain atoms b and c in Fig. 7. Even though we cannot assign these components to individual atoms (i.e., to either b or c), we suppose the bonding configurations and charge states of the b and c atoms to be different. The difference can be explained in terms of the buckling of the Ge=Ge double bond in the Yb/Ge HCC structure, as shown in Fig. 7, and should result in a difference in core-level binding energy, as was already found, for example, for the Si(100)- (2×1) and Ge(100)- (2×1) surfaces with buckled dimers.⁵⁸ The buckling was not observed for the Si and Ge HCC (3×2) surfaces previously, and this suggestion calls for further verification by other experimental and theoretical techniques. We note, however, that “slow” experimental techniques, such as STM, might not visualize the buckling of the Ge HCC substrate if there is a rapid vertical motion (dynamical fluctuation) of the b and c atoms. For this reason, the STM imaging is desirable at low temperature at which the dynamical fluctuation can be frozen out.

It is worth noting that the intensity ratio of the $S3$ and $S4$ components (2:1) does not fit the number ratio of b and c atoms (1:1). Also, the intensity ratio of $S2:(S3+S4)$, which is about 4:3, does not correspond to the atomic ratio of $(a+d):(b+c)=1:1$ precisely. We assume that some of the second-layer Ge atoms may affect the $S2$ and $S3$ intensities, while more prominently shifted second-layer atoms give rise to the $S1$ component. This suggests that the second-layer substrate atoms in the Yb/Ge(111)- (3×2) contribute more strongly to core-level spectra than those of the Eu/Ge(111)- $(3 \times 2)/(3 \times 4)$ and Si (3×2) HCC reconstructions. Therefore, based on the present results, the HCC reconstruction of the Yb/Ge(111)- (3×2) phase implies a

more drastic rearrangement of the Ge substrate, which leads to the buckling of the Ge=Ge double bond in the top layer, and also has a more pronounced effect on the second-layer atoms.

V. CONCLUSIONS

In conclusion, we have investigated the 1/6 ML Yb/Ge(111)- (3×2) surface by LEED and high-resolution photoelectron spectroscopy. LEED patterns exhibit a clear (3×1) periodicity without half-order features, but this is still associated with a (3×2) structure in real space, as explained in the literature (e.g., see Ref. 44). The Yb $4f$ spectrum of Yb/Ge(111)- (3×2) consists of a single component corresponding to divalent Yb atoms. This implies that the metal atoms reside at equivalent adsorption sites in the Yb/Ge(111)- (3×2) reconstruction. No emission was found at the Fermi level, indicating the semiconducting nature of the Yb/Ge(111)- (3×2) surface. Five surface components with SCLS of $-0.19(S1)$, $-0.38(S2)$, $0.22(S3)$, $0.52(S4)$, and 0.82 eV ($S5$) relative to the bulk emission were identified in Ge $3d$ spectra from the Yb/Ge(111)- (3×2) surface. The first four components were shown to be related to the Yb/Ge reconstruction, and the latter is due to defects. Of the $S1$ – $S4$ components, the $S2$ – $S4$ predominantly originate from the top-layer Ge atoms of Yb/Ge(111)- (3×2) , while $S1$ is due to the emission from the subsurface layer(s). Based on our findings, we propose a HCC-like atomic model with a buckled Ge=Ge double bond and the Yb atoms adsorbed at $T4$ sites. Also, in contrast to Si (3×2) reconstructions, the second Ge layer is expected to be more dramatically rearranged. This difference might be due to the individual properties of REM-Ge and REM-Si bonds in the (3×2) HCC reconstructions.

ACKNOWLEDGMENTS

We are grateful to H. Ollila and the MAX-lab staff for technical assistance. We thank H. Karhu for providing valuable comments on software. The financial support by the Transnational Access to the Research Infrastructure Program (TARI) is acknowledged. This work has been supported in part by the Academy of Finland Grant No. 205766 (I.J.V.). K.S. acknowledges support from the Anne McLaren Foundation from the University of Nottingham.

*Permanent address: A. F. Ioffe Physico-Technical Institute, Russian Academy of Sciences, 194021 St. Petersburg, Russian Federation. Electronic address: m.kuzmin@mail.ioffe.ru

¹J. R. Ahn, N. D. Kim, S. S. Lee, K. D. Lee, B. D. Yu, D. Jeon, K. Kong, and J. W. Chung, Europhys. Lett. **57**, 859 (2002).

²P. Segovia, P. Purdie, M. Hengsberger, and Y. Baer, Nature (London) **402**, 504 (1999).

³H. W. Yeom, S. Takeda, E. Rotenberg, I. Matsuda, K. Horikoshi, J. Schaefer, C. M. Lee, S. D. Kevan, T. Ohta, T. Nagao, and S. Hasegawa, Phys. Rev. Lett. **82**, 4898 (1999).

⁴J. M. Carpinelli, H. H. Weitering, E. W. Plummer, and R. Stumpf, Nature (London) **381**, 398 (1996).

⁵R. Losio, K. N. Altmann, A. Kirakosian, J.-L. Lin, D. Y. Petrovykh, and F. J. Himpsel, Phys. Rev. Lett. **86**, 4632 (2001).

⁶C. Collazo-Davila, D. Grozea, and L. D. Marks, Phys. Rev. Lett. **80**, 1678 (1998).

⁷L. Lottermoser, E. Landemark, D.-M. Smilgies, M. Nielsen, R. Feidenhans'l, G. Falkenberg, R. L. Johnson, M. Gierer, A. P. Seitsonen, H. Kleine, H. Bludau, H. Over, S. K. Kim, and F. Jona, Phys. Rev. Lett. **80**, 3980 (1998).

- ⁸Steven C. Erwin and Hanno H. Weitering, *Phys. Rev. Lett.* **81**, 2296 (1998).
- ⁹Myung-Ho Kang, Jin-Ho Kang, and Sukmin Jeong, *Phys. Rev. B* **58**, R13359 (1998).
- ¹⁰H. H. Weitering, X. Shi, and S. C. Erwin, *Phys. Rev. B* **54**, 10585 (1996); K. Sakamoto, T. Okuda, H. Nishimoto, H. Daimon, S. Suga, T. Kinoshita, and A. Kakizaki, *ibid.* **50**, 1725 (1994); T. Okuda, K. Sakamoto, H. Nishimoto, H. Daimon, S. Suga, T. Kinoshita, and A. Kakizaki, *ibid.* **55**, 6762 (1997).
- ¹¹Shigehiko Hasegawa, Masakatsu Maruyama, Yoshitane Hirata, Daisuke Abe, and Hisao Nakashima, *Surf. Sci.* **405**, L503 (1998); O. Kubo, A. A. Saranin, A. V. Zotov, J.-T. Ryu, H. Tani, T. Harada, M. Katayama, V. G. Lifshits, and K. Oura, *ibid.* **415**, L415 (1998); A. A. Saranin, A. V. Zotov, V. G. Lifshits, J.-T. Ryu, O. Kubo, H. Tani, T. Harada, M. Katayama, and K. Oura, *Phys. Rev. B* **58**, 3545 (1998).
- ¹²Ji Young Lee and Myung-Ho Kang, *Phys. Rev. B* **66**, 233301 (2002).
- ¹³Geunseop Lee, Jonggeol Kim, I. Chizhov, H. Mai, and R. F. Willis, *Phys. Rev. B* **61**, 9921 (2000); Myonggeun Yoon, H. Mai, Geunseop Lee, and R. F. Willis, *Surf. Sci.* **463**, 183 (2000).
- ¹⁴Geunseop Lee, Jonggeol Kim, H. Mai, Ilya Chizhov, and R. F. Willis, *J. Vac. Sci. Technol. A* **18**, 1488 (2000).
- ¹⁵Geunseop Lee, H. Mai, and R. F. Willis, *Phys. Rev. B* **63**, 085323 (2001).
- ¹⁶Geunseop Lee, Suklyun Hong, Hanchul Kim, Dongsoo Shin, Ja-Yong Koo, Hyung-Ik Lee, and Dae Won Moon, *Phys. Rev. Lett.* **87**, 056104 (2001).
- ¹⁷A. A. Baski, S. C. Erwin, M. S. Turner, K. M. Jones, J. W. Dickinson, and J. A. Carlisle, *Surf. Sci.* **476**, 22 (2001).
- ¹⁸Geunseop Lee, Suklyun Hong, Hanchul Kim, and Ja-Yong Koo, *Phys. Rev. B* **68**, 115314 (2003).
- ¹⁹Frank Palmino, Eric Ehret, Louay Mansour, Jean-Claude Labrune, Geunseop Lee, Hanchul Kim, and Jean-Marc Themlin, *Phys. Rev. B* **67**, 195413 (2003).
- ²⁰E. Ehret, F. Palmino, L. Mansour, E. Duverger, and J.-C. Labrune, *Surf. Sci.* **569**, 23 (2004).
- ²¹T. Sekiguchi, F. Shimokoshi, T. Nagao, and S. Hasegawa, *Surf. Sci.* **493**, 148 (2001).
- ²²Kazuyuki Sakamoto, Wakaba Takeyama, H. M. Zhang, and R. I. G. Uhrberg, *Phys. Rev. B* **66**, 165319 (2002).
- ²³Kazuyuki Sakamoto, H. M. Zhang, and R. I. G. Uhrberg, *Phys. Rev. B* **69**, 125321 (2004); K. Sakamoto, A. Pick, and R. I. G. Uhrberg, *ibid.* **72**, 045310 (2005); Shinya Takada, Kazuyuki Sakamoto, Keisuke Kobayashi, Toshihiro Suzuki, Ayumi Harasawa, Taichi Okuda, and Toyohiko Kinoshita, *Appl. Surf. Sci.* **252**, 5292 (2006).
- ²⁴M. Kuzmin, R.-L. Vaara, P. Laukkanen, R. E. Perälä, and I. J. Väyrynen, *Surf. Sci.* **538**, 124 (2003).
- ²⁵M. Kuzmin, P. Laukkanen, R. E. Perälä, R.-L. Vaara, and I. J. Väyrynen, *Phys. Rev. B* **71**, 155334 (2005).
- ²⁶Kazuyuki Sakamoto, A. Pick, and R. I. G. Uhrberg, *Phys. Rev. B* **72**, 195342 (2005).
- ²⁷T. Okuda, K.-S. An, A. Harasawa, and T. Kinoshita, *Phys. Rev. B* **71**, 085317 (2005).
- ²⁸R. H. Miwa, *Phys. Rev. B* **72**, 085325 (2005).
- ²⁹Suklyun Hong, Geunseop Lee, and Hanchul Kim, *J. Korean Phys. Soc.* **47**, 100 (2005).
- ³⁰M. Kuzmin, P. Laukkanen, R. E. Perälä, and I. J. Väyrynen, *Phys. Rev. B* **73**, 125332 (2006).
- ³¹M. Kuzmin, R. E. Perälä, P. Laukkanen, M. Ahola-Tuomi, and I. J. Väyrynen, *Phys. Rev. B* **74**, 115320 (2006).
- ³²T. Okuda, H. Shigeoka, H. Daimon, S. Suga, T. Kinoshita, and A. Kakizaki, *Surf. Sci.* **321**, 105 (1994).
- ³³J. J. Paggel, G. Neuhold, H. Haak, and K. Horn, *Phys. Rev. B* **52**, 5813 (1995).
- ³⁴M.-H. Kang, J.-H. Kang, and S. Jeong, *Phys. Rev. B* **58**, R13359 (1998).
- ³⁵M. Gurnett, J. B. Gustafsson, L. J. Holleboom, K. O. Magnusson, S. M. Widstrand, L. S. O. Johansson, M. K.-J. Johansson, and S. M. Gray, *Phys. Rev. B* **71**, 195408 (2005).
- ³⁶M. Göthelid, S. Odasso, G. LeLay, M. Björkqvist, E. Janin, U. O. Karlsson, and T. M. Grehk, *Surf. Sci.* **104/105**, 113 (1996).
- ³⁷J. W. Kim, S. Kim, J. M. Seo, S. Tanaka, and M. Kamada, *J. Phys.: Condens. Matter* **10**, 3731 (1998).
- ³⁸T. M. Grehk, M. Göthelid, M. Björkqvist, G. Le Lay, and U. O. Karlsson, *Phys. Rev. B* **61**, 4963 (2000).
- ³⁹C. Wigren, J. N. Andersen, R. Nyholm, U. O. Karlsson, J. Nogami, A. A. Baski, and C. F. Quate, *Phys. Rev. B* **47**, 9663 (1993).
- ⁴⁰C. Wigren, J. N. Andersen, R. Nyholm, M. Göthelid, M. Hammar, C. Törnevik, and U. O. Karlsson, *Phys. Rev. B* **48**, 11014 (1993).
- ⁴¹<http://maxsun5.maxlab.lu.se/beamlines/bl33/>
- ⁴²M. Kuzmin, R.-L. Vaara, P. Laukkanen, R. E. Perälä, and I. J. Väyrynen, *Surf. Sci.* **549**, 183 (2004).
- ⁴³H. H. Weitering, *Surf. Sci.* **355**, L271 (1996).
- ⁴⁴J. Schäfer, S. C. Erwin, M. Hansmann, Z. Song, E. Rotenberg, S. D. Kevan, C. S. Hellberg, and K. Horn, *Phys. Rev. B* **67**, 085411 (2003).
- ⁴⁵R.-L. Vaara, M. Kuzmin, R. E. Perälä, P. Laukkanen, and I. J. Väyrynen, *Surf. Sci.* **529**, L229 (2003).
- ⁴⁶J. R. Chelikowsky and M. L. Cohen, *Phys. Rev. B* **14**, 556 (1976).
- ⁴⁷R. D. Bringans and H. Höchst, *Phys. Rev. B* **25**, 1081 (1982).
- ⁴⁸T. Yokotsuka, S. Kono, S. Suzuki, and T. Sagawa, *J. Phys. Soc. Jpn.* **53**, 696 (1984).
- ⁴⁹A. L. Wachs, T. Miller, T. C. Hsieh, A. P. Shapiro, and T.-C. Chiang, *Phys. Rev. B* **32**, 2326 (1985).
- ⁵⁰J. M. Nicholls, G. V. Hansson, R. I. G. Uhrberg, and S. A. Flodström, *Phys. Rev. B* **33**, 5555 (1986).
- ⁵¹R. D. Bringans, R. I. G. Uhrberg, and R. Z. Bachrach, *Phys. Rev. B* **34**, 2373 (1986).
- ⁵²J. Aarts, A. J. Hoeven, and P. K. Larsen, *Phys. Rev. B* **37**, 8190 (1988).
- ⁵³Noboru Takeuchi, A. Selloni, and E. Tosatti, *Phys. Rev. Lett.* **69**, 648 (1992).
- ⁵⁴F. Gerken, *J. Phys. F: Met. Phys.* **13**, 703 (1983).
- ⁵⁵M. E. Davila, S. L. Molodtsov, C. Laubschat, and M. C. Asensio, *Phys. Rev. B* **66**, 035411 (2002).
- ⁵⁶H. W. Yeom, T. Abukawa, Y. Takakuwa, S. Fujimori, T. Okane, Y. Ogura, T. Miura, S. Sato, A. Kakizaki, and S. Kono, *Surf. Sci.* **395**, L236 (1998).
- ⁵⁷M. Göthelid, T. M. Grehk, M. Hammar, U. O. Karlsson, and S. A. Flodström, *Phys. Rev. B* **48**, 2012 (1993).
- ⁵⁸E. Landemark, C. J. Karlsson, Y.-C. Chao, and R. I. G. Uhrberg, *Phys. Rev. Lett.* **69**, 1588 (1992); R. Cao, X. Yang, J. Terry, and P. Pianetta, *Phys. Rev. B* **45**, 13749 (1992); E. Pehlke and M. Scheffler, *Phys. Rev. Lett.* **71**, 2338 (1993).